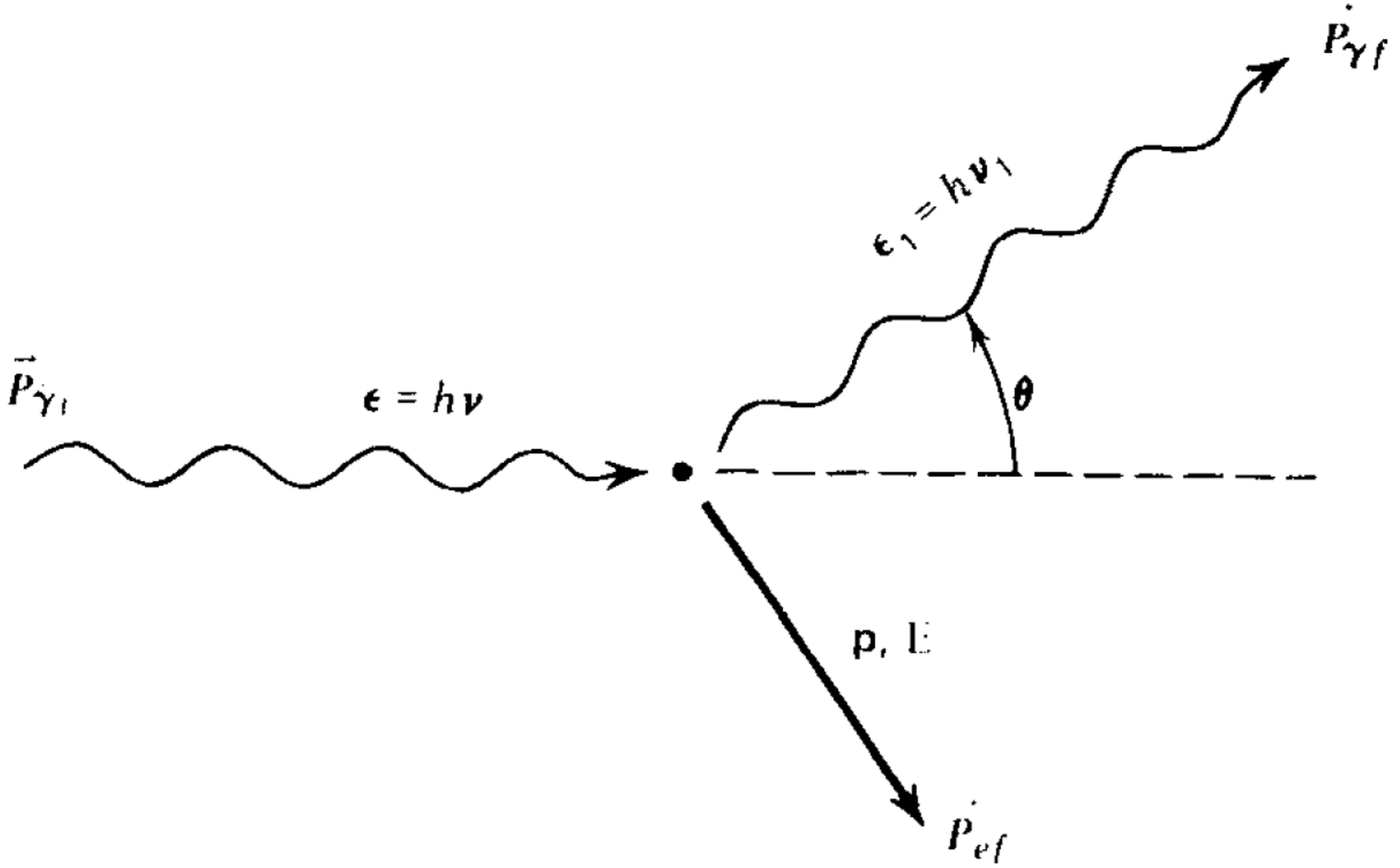

Figure 7.1 Geometry for scattering of a photon by an electron initially at rest.

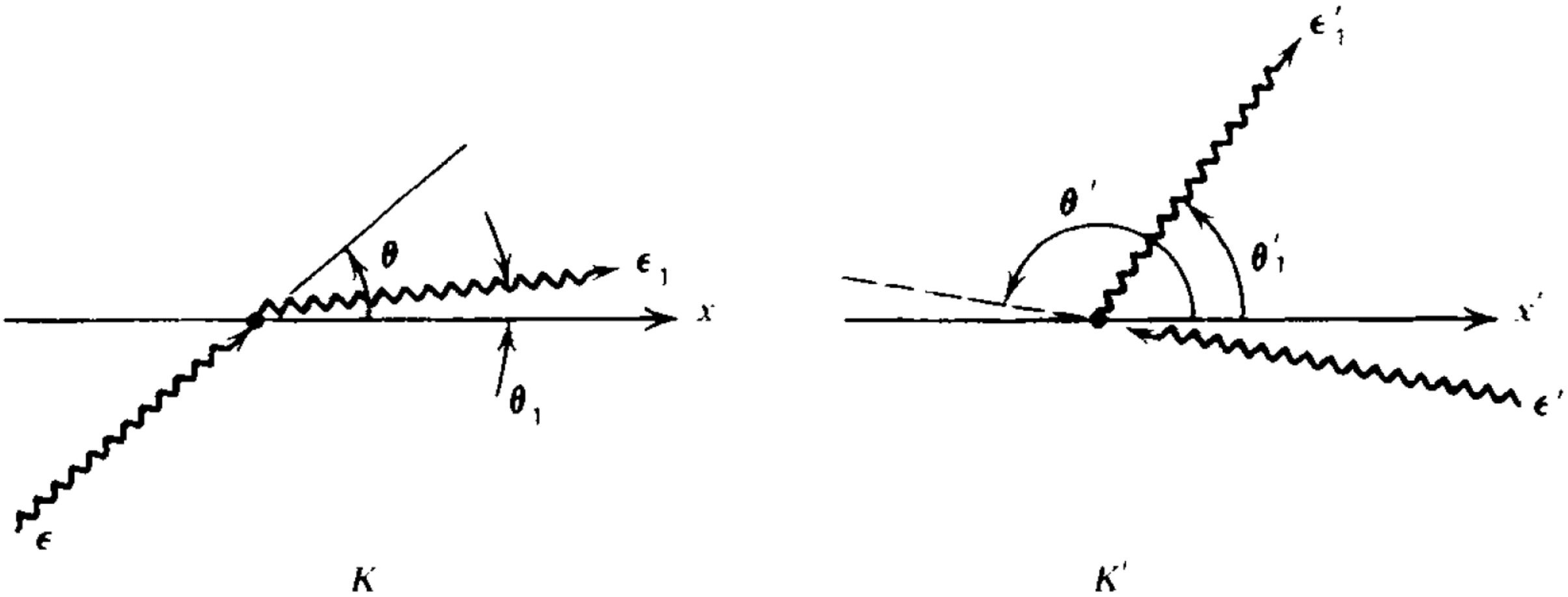

Figure 7.2 Scattering geometries in the observer's frame K and in the electron rest frame K′.

Sunyaev-Zeldovich Effect

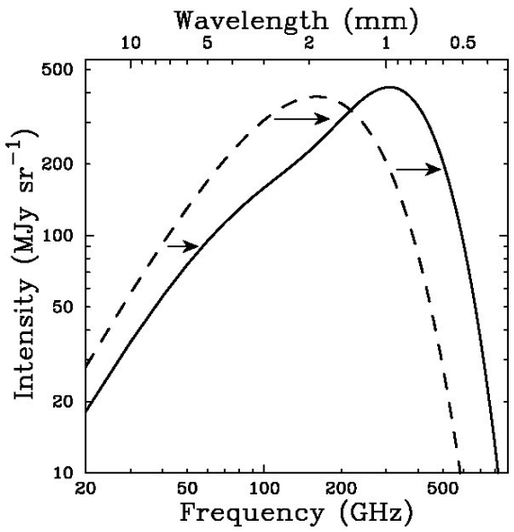

Inverse Compton scattering of CMB photons off the ICM electrons

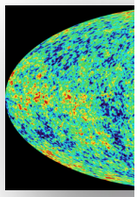

➔ Signal virtually independent of redshift

➔ Proportional to the l.o.s. integration of $n_e T_e \sim$ pressure

➔ Wider dynamic range accessible

➔ We are now in the era of SZ cluster cosmology (e.g. ACT, SPT, Planck)

Coma as seen by Planck

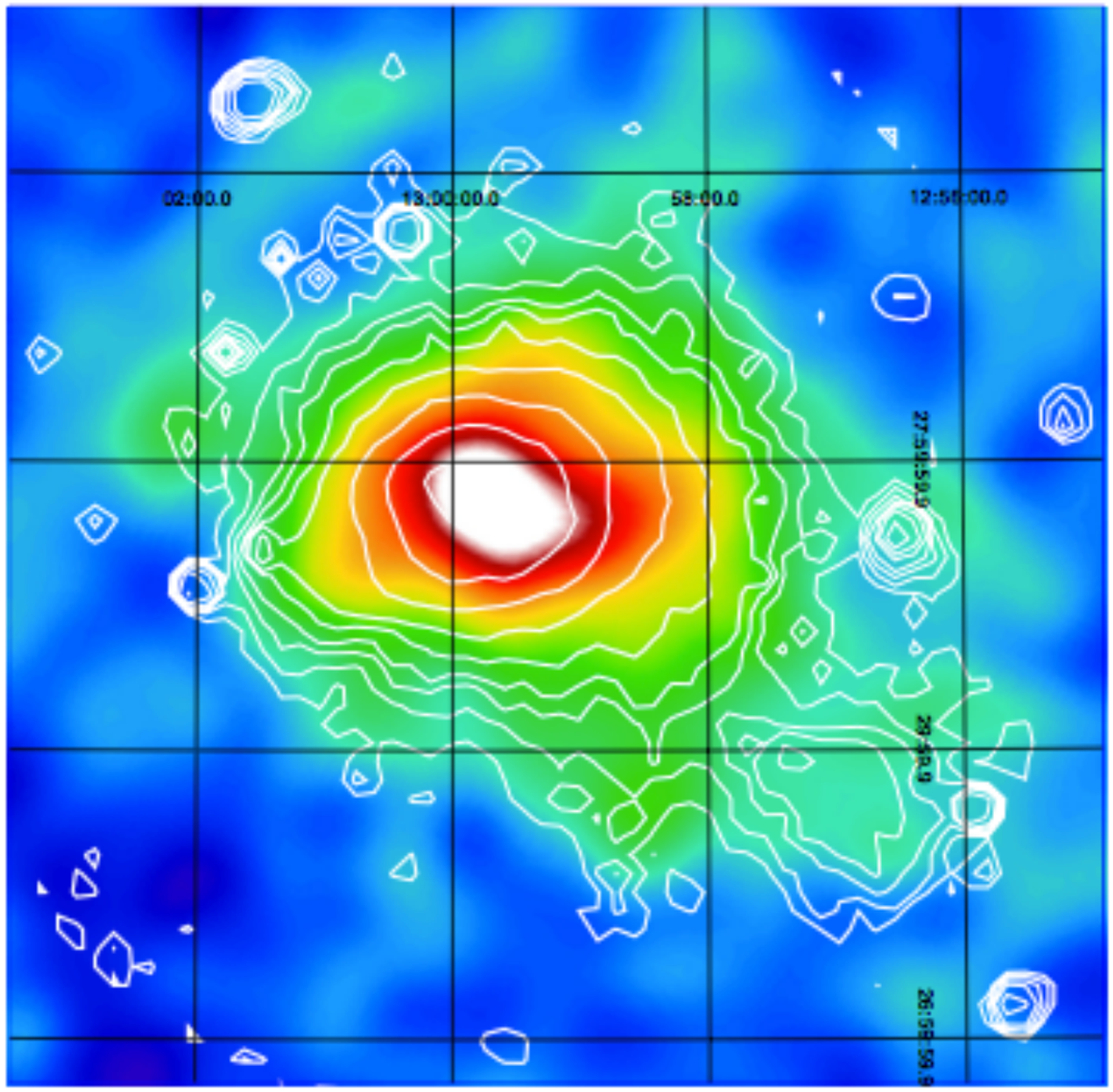

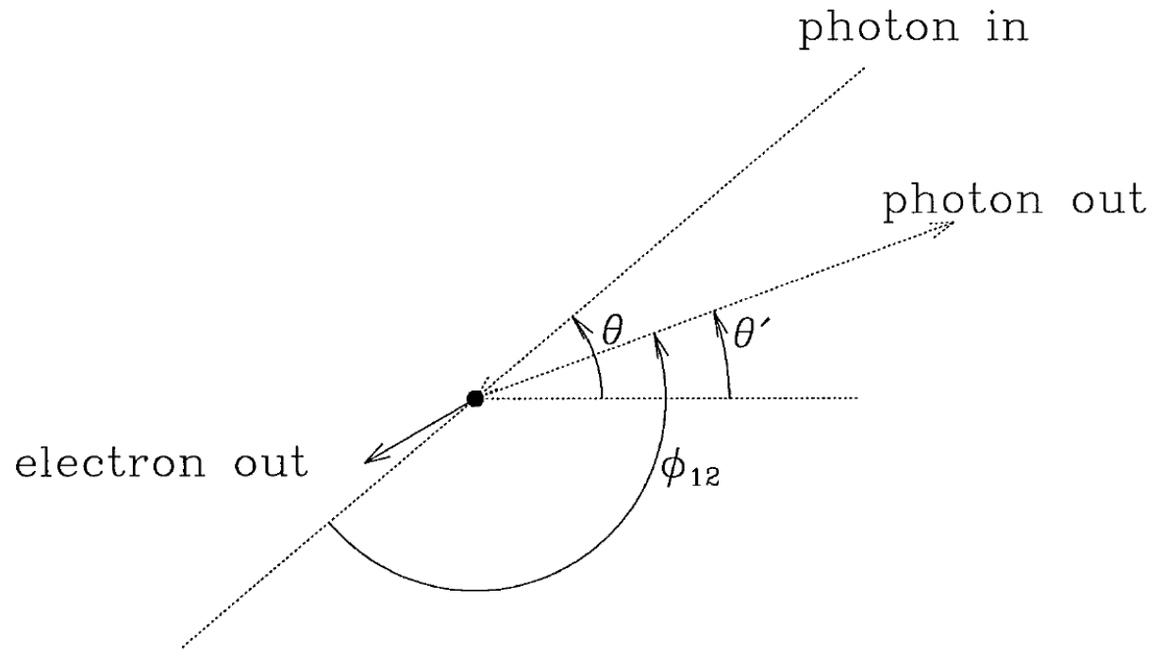

Fig. 3. The scattering geometry, in the frame of rest of the electron before the interaction. An incoming photon, at angle θ relative to the x_e axis, is deflected by angle ϕ_{12}, and emerges after the scattering at angle θ' with almost unchanged energy (Eq. (21)). In the observer's frame, where the electron is moving with velocity βc along the x_e axis, the photon changes energy by an amount depending on β and the angles θ and θ' (Eq. (25)).

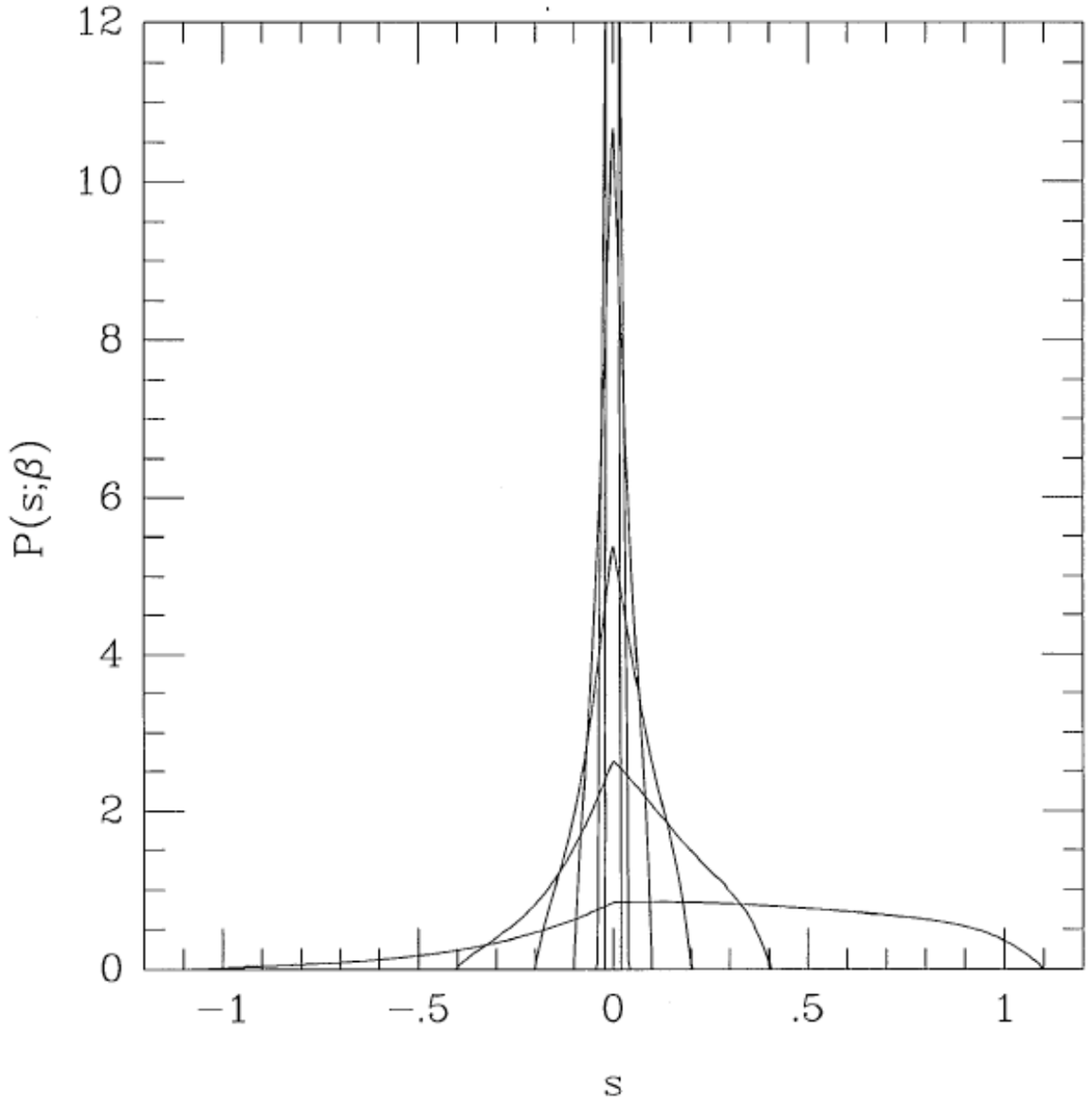

Fig. 4. The scattering probability function $P(s;\beta)$, for $\beta = 0.01, 0.02, 0.05, 0.10, 0.20$, and 0.50. The function becomes increasingly asymmetric and broader as β increases.

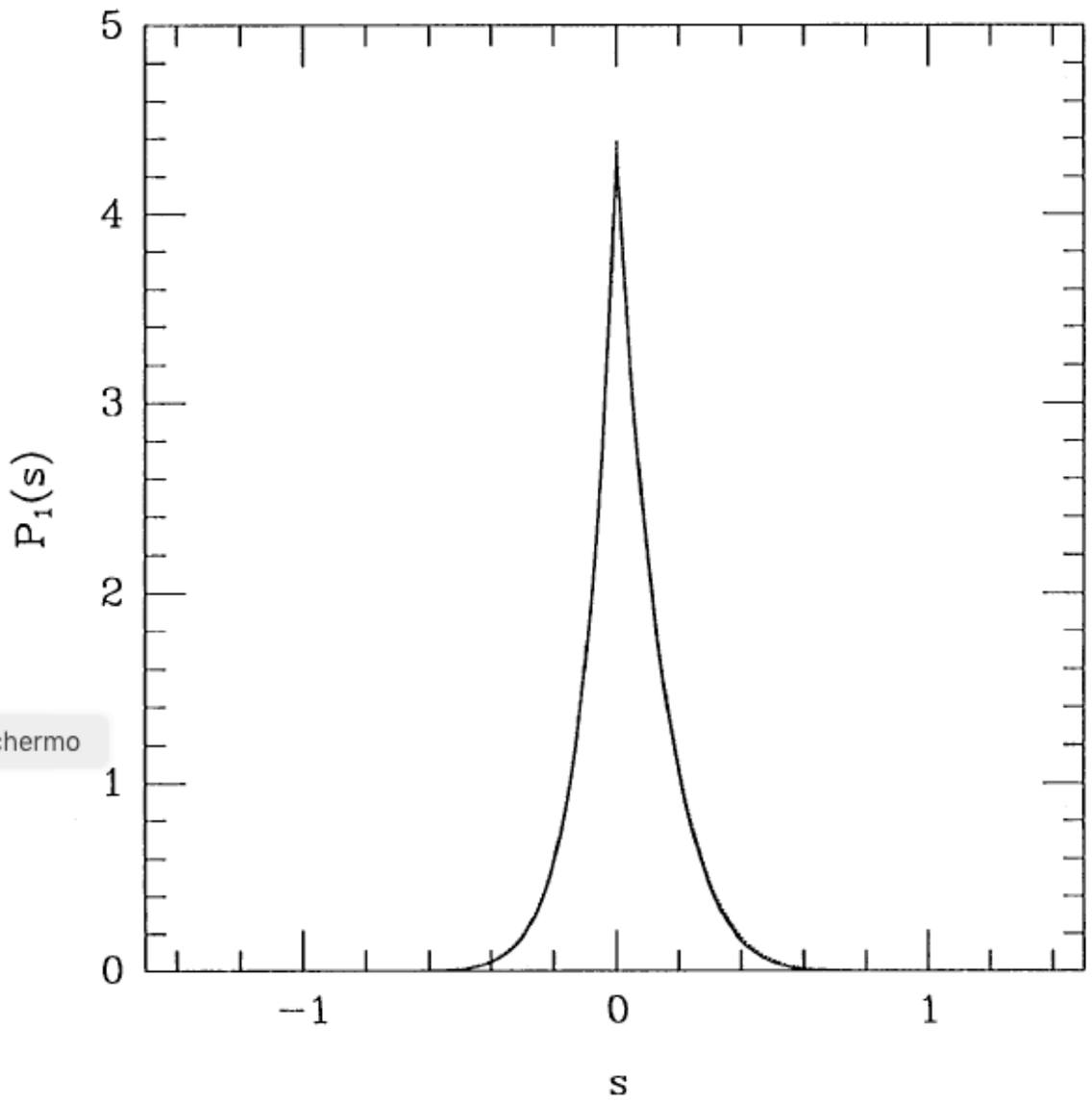

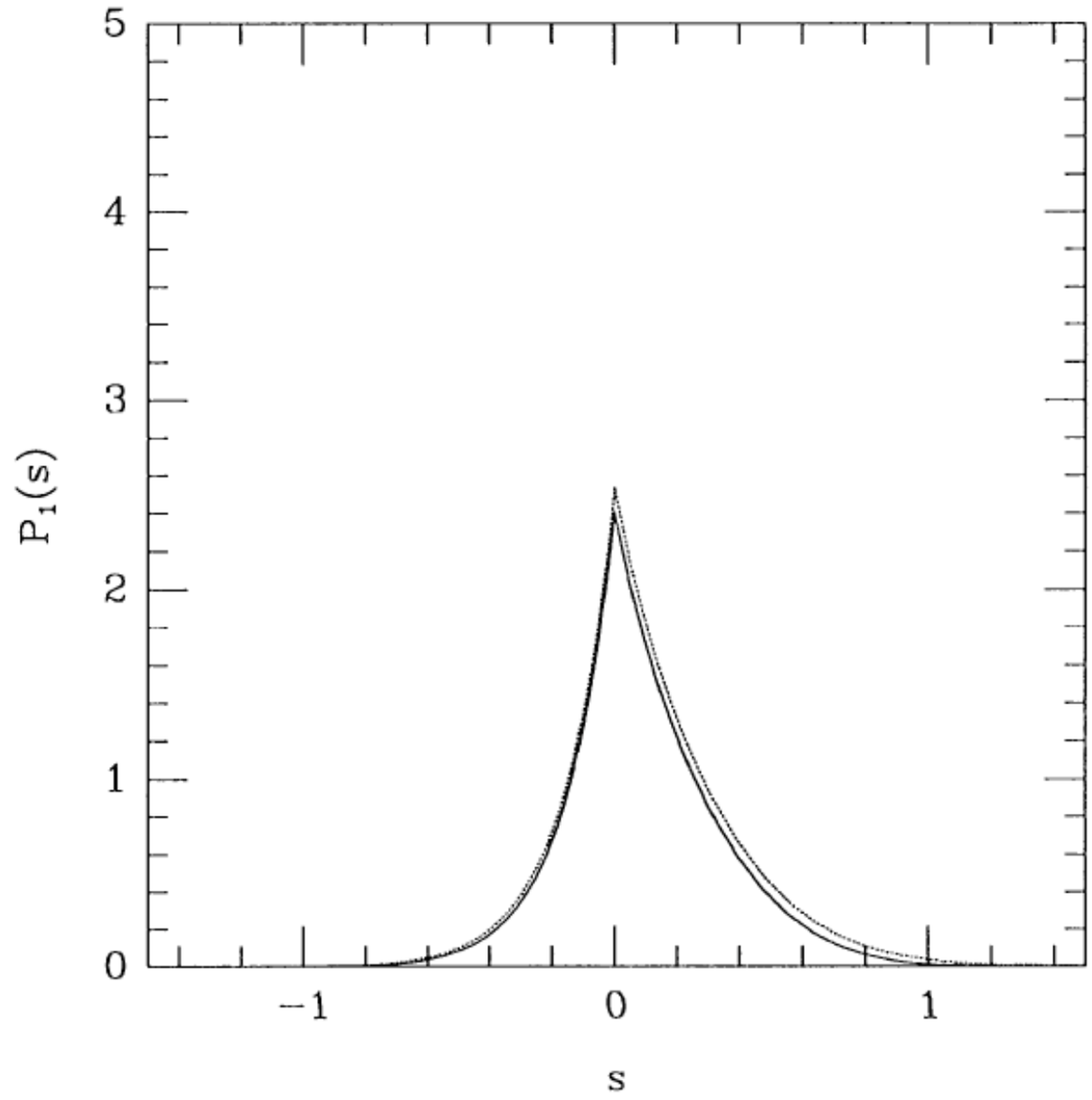

Fig. 5. The scattering kernel, $P_1(s)$, for gases at 5.1 and 15.3 keV. The solid line shows the scattering kernels calculated according to Eq. (33), as derived by Rephaeli (1995a). The dotted line indicates the scattering kernels as calculated by Sunyaev (1980), based on the results of Babuel-Payrissac and Rouvillois (1969).

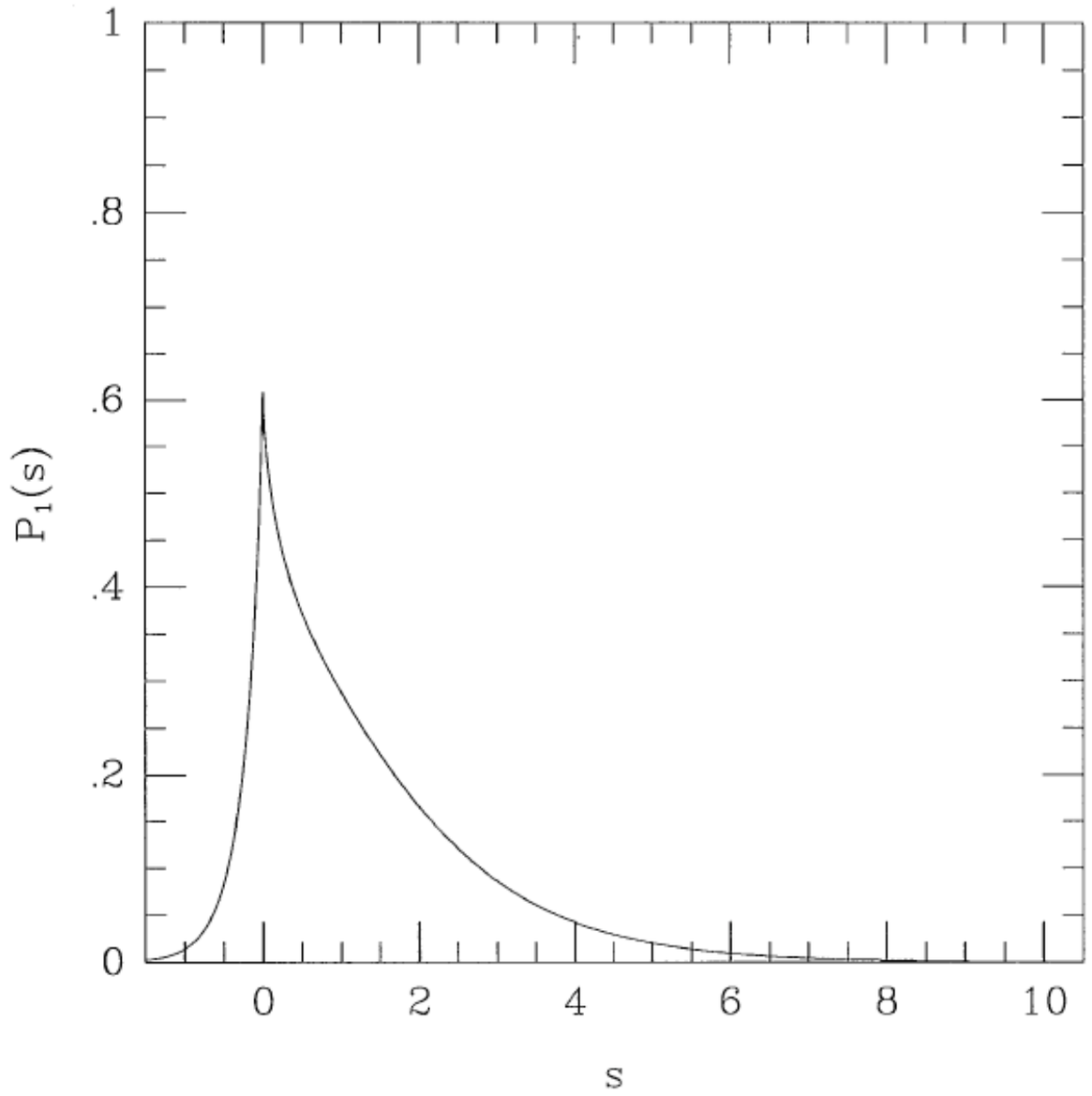

Fig. 6. The scattering kernel, $P_1(s)$, for a power-law electron distribution with energy index $\alpha = 2.5$ (see Eq. (37)). The stronger upscattering tail here, relative to Fig. 5, is caused by the higher proportion of fast electrons in distribution (37) than (35).

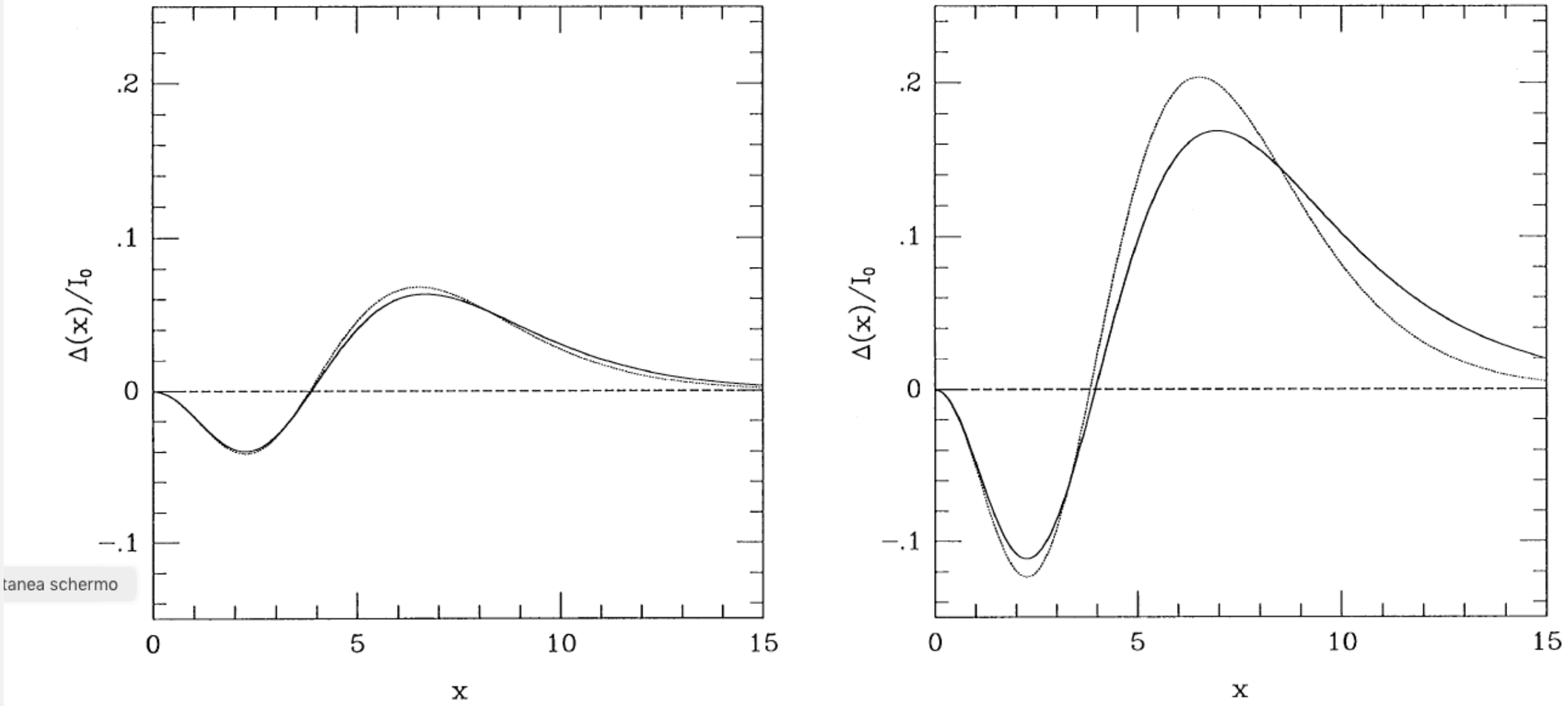

Fig. 7. The spectral deformation caused by inverse-Compton scattering of an incident Planck spectrum after a single scattering from a thermal population of electrons as a function of dimensionless frequency $x = h\nu/k_B T_{rad} = 0.0176(\nu/\mathrm{GHz})$, with scaling $I_0 = (2h/c^2)(k_B T_{rad}/h)^3$. Left, for electrons at $k_B T_e = 5.1\,\mathrm{keV}$; right for electrons at $k_B T_e = 15.3\,\mathrm{keV}$. The result obtained from the Kompaneets kernel is shown as a dotted line. The shape of the distortion is independent of T_e (and the amplitude is proportional to T_e) for the Kompaneets kernel, but the relativistic expression leads to a more complicated form.

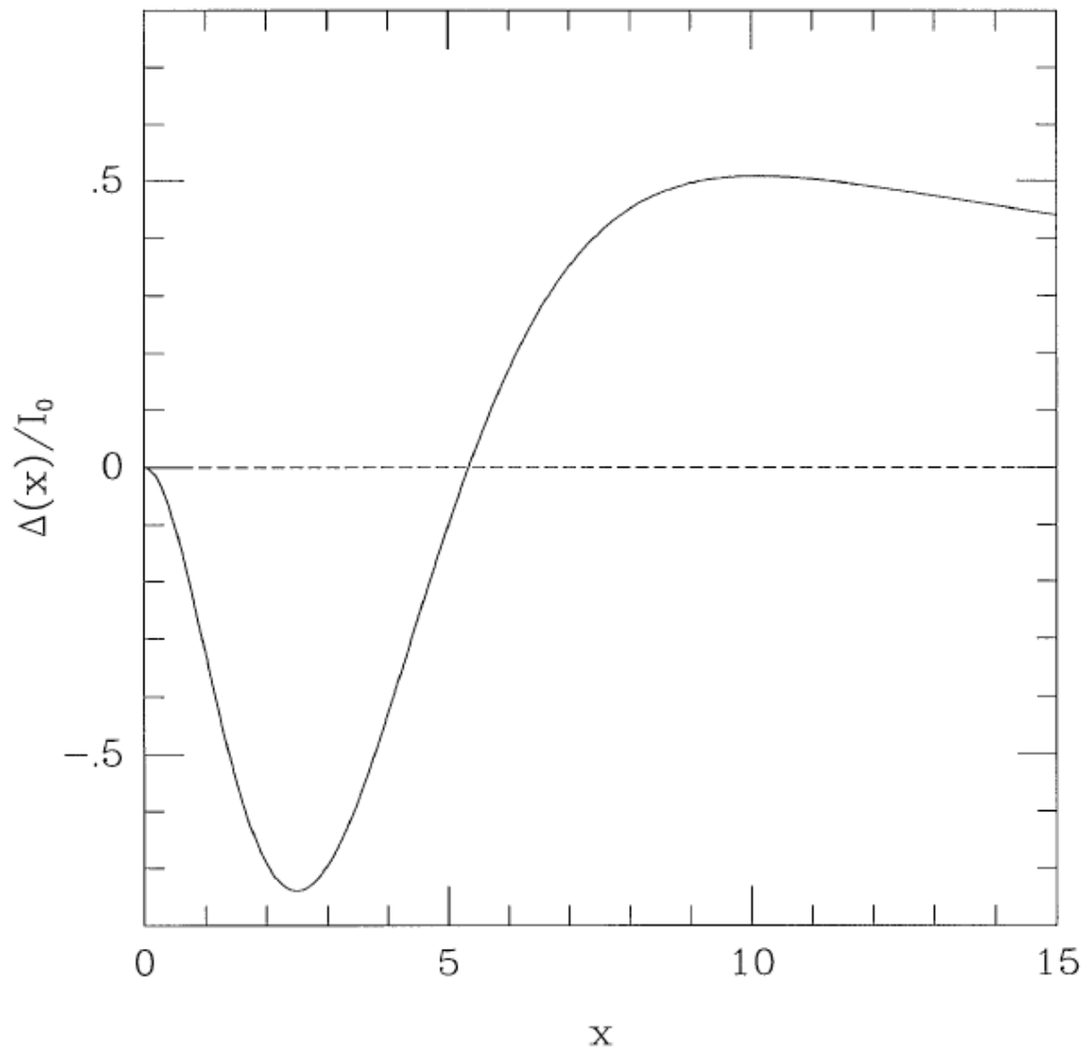

Fig. 8. The fractional spectral deformation caused by inverse-Compton scattering of an incident Planck spectrum by a single scattering from a power-law population of electrons with $\alpha = 2.5$ (Eq. (37)). The spectral deformation has a similar shape to that seen in Fig. 7, but with a deeper minimum and more extended tail. This arises from the larger frequency shifts caused by the higher Lorentz factors of the electrons (see Fig. 6).

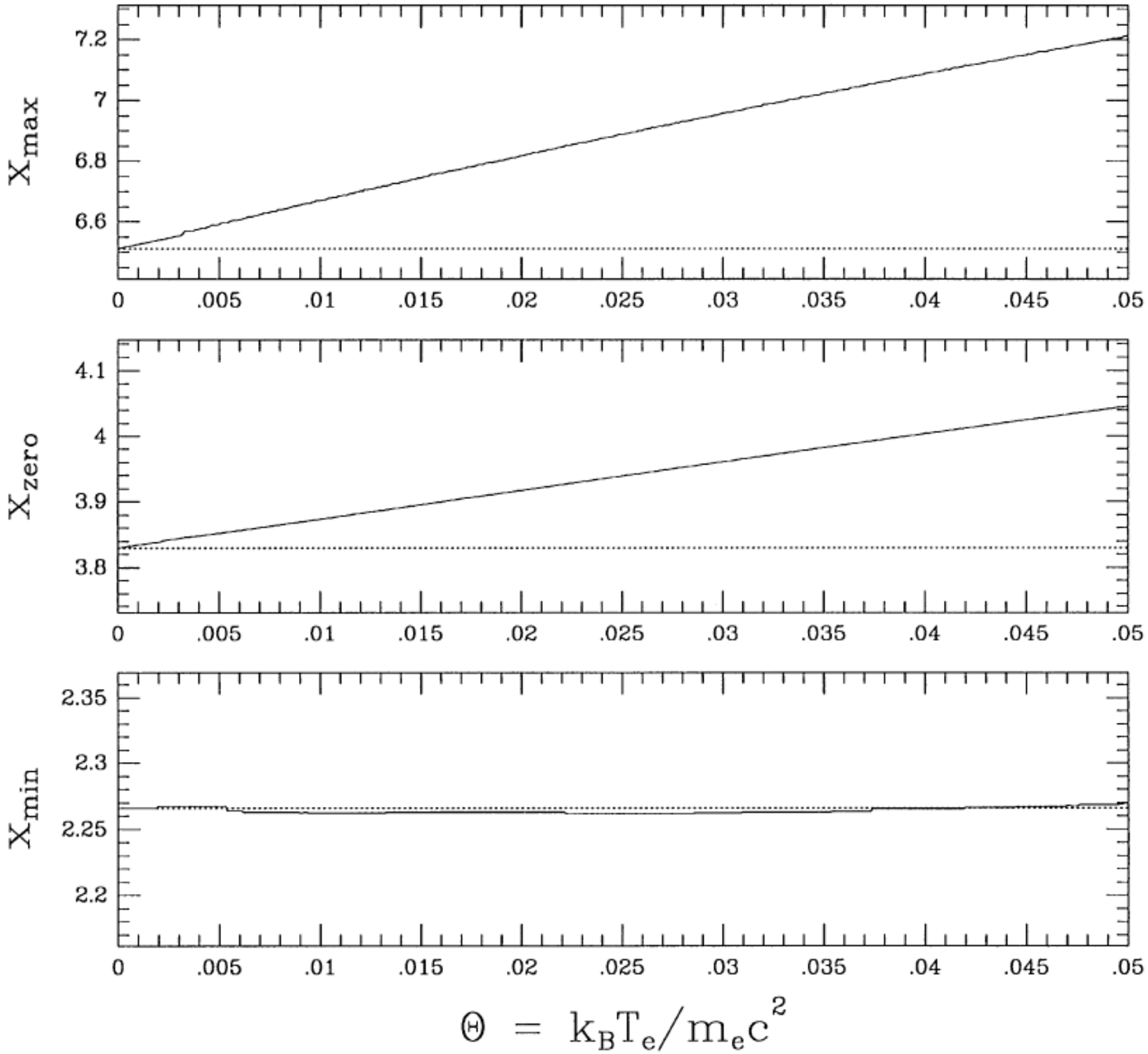

Fig. 9. The variation of the positions of the minimum, zero, and maximum of the spectrum of the thermal Sunyaev–Zel'dovich effect, $\Delta I(x)$, as the electron temperature varies. The positions of the spectral features are described by the dimensionless frequency $x = h\nu/k_B T_{rad}$, and the electron temperature is characterized by $\Theta = k_B T_e/m_e c^2$.

Inverse Compton & thermal SZ

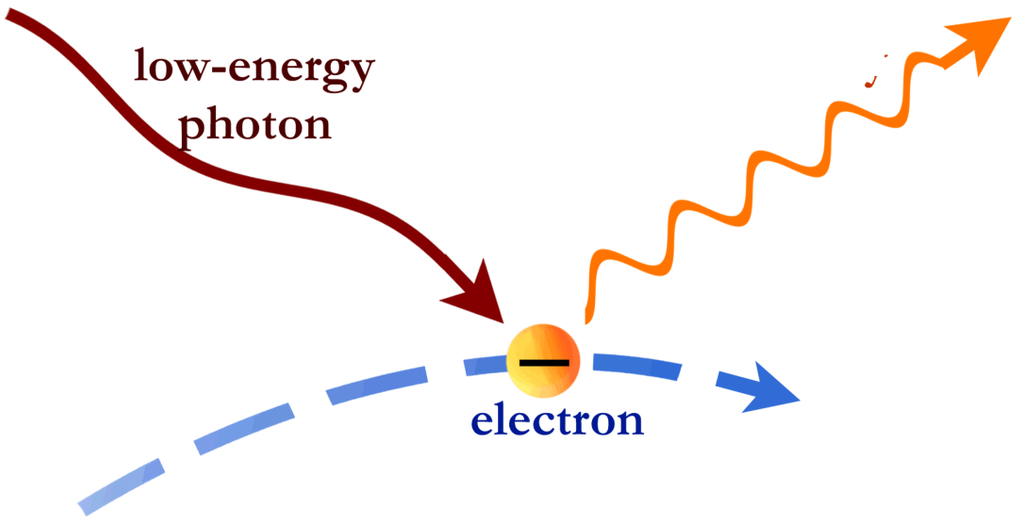

See lectures by R. Sunyaev

Kompaneets equation: describes the variation of the photon frequency distribution $n(\nu)$ due to single IC-scattering on a population of thermal electrons with temperature T_e, in the non-relativistic regime $k_B T_e \ll m_e c^2$

$$\frac{\partial n}{\partial y} = \frac{1}{x_e^2}\frac{\partial}{\partial x_e} x_e^4 \left(\frac{\partial n}{\partial x_e} + n + n^2 \right) \qquad x_e = h\nu / k_B T_e$$

$$y = \frac{k_B T_e}{m_e c^2}\frac{c\,t}{\lambda_e}$$

➔ Compton-y parameter: average fractional energy change per scattering times mean number of scatterings

➔ $\lambda_e = (n_e \sigma_T)^{-1}$: scattering mean free path

$$y = \int n_e \, \sigma_T \, dl \, \frac{k_B T_e}{m_e c^2}$$

$x_e \ll 1$ ➔ $\frac{\partial n}{\partial x_e} \gg n,\ n^2$ ➔ $\frac{\partial n}{\partial y} = \frac{1}{x_e^2}\frac{\partial}{\partial x_e} x_e^4 \frac{\partial n}{\partial x_e}$: diffusion equation

Inverse Compton & thermal SZ

$$\frac{\partial n}{\partial y} = \frac{1}{x_{\rm e}^2}\frac{\partial}{\partial x_{\rm e}} x_{\rm e}^4 \frac{\partial n}{\partial x_{\rm e}}$$

Take advantage of the homogeneity of this equation to replace $x_{\rm e}$ with $x = h\nu/k_{\rm B}T_{\rm rad}$

For $y \ll 1$ (~10^{-4} in clusters), for a Black Body incident spectrur $n_\alpha = \left(e^{h\nu/k_{\rm B}T_{\rm rad}} - 1\right)^{-1}$

and using $\frac{\partial n}{\partial y} = \frac{\Delta n}{y}$ ➔

$$\Delta n = x\, y \frac{e^x}{(e^x-1)^2}\left(x\,\coth(x/2) - 4\right)$$

Variation of specific intensity:

$$\Delta I(x) = x^3 \Delta n(x) I_0$$

$$I_0 = \frac{2h}{c^2}\left(\frac{k_{\rm B}T_{\rm rad}}{h}\right)^3$$

Amplitude of distortion provides
l.o.s. integral of the ICM pressure

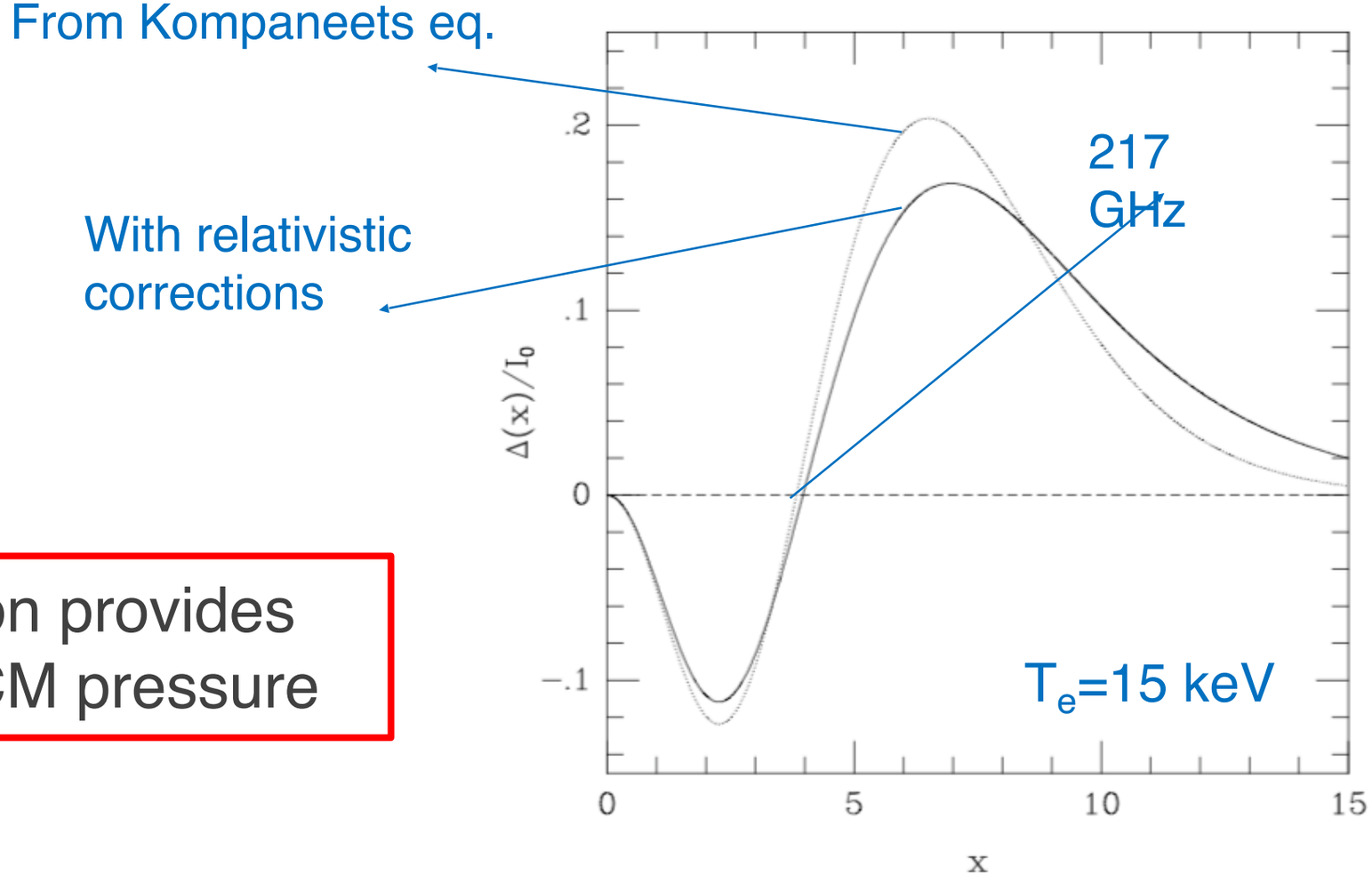

The thermal SZ effect

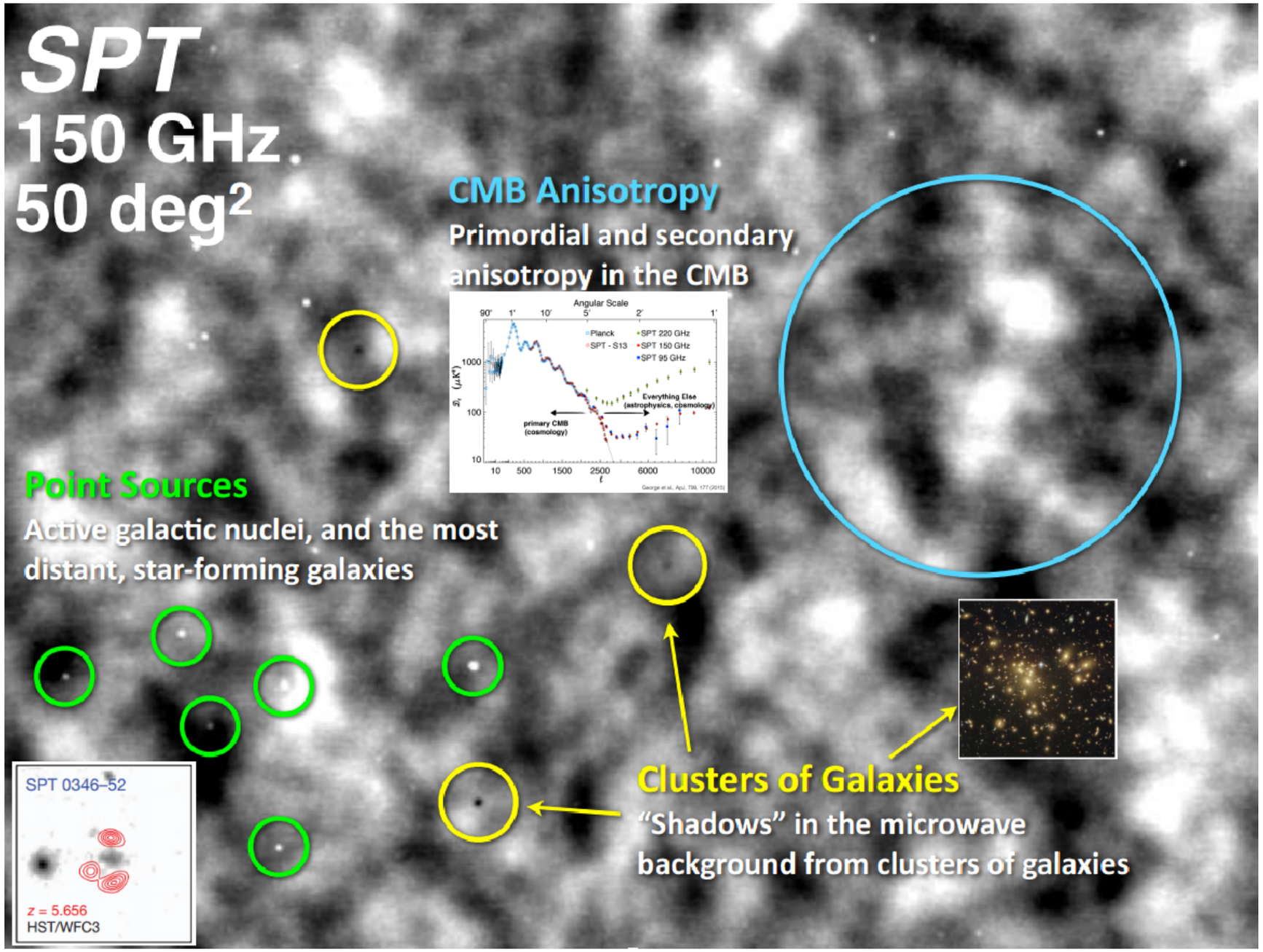

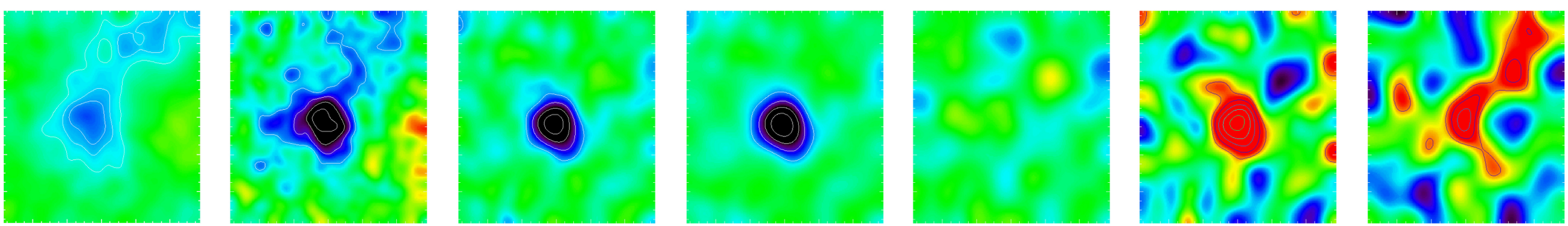

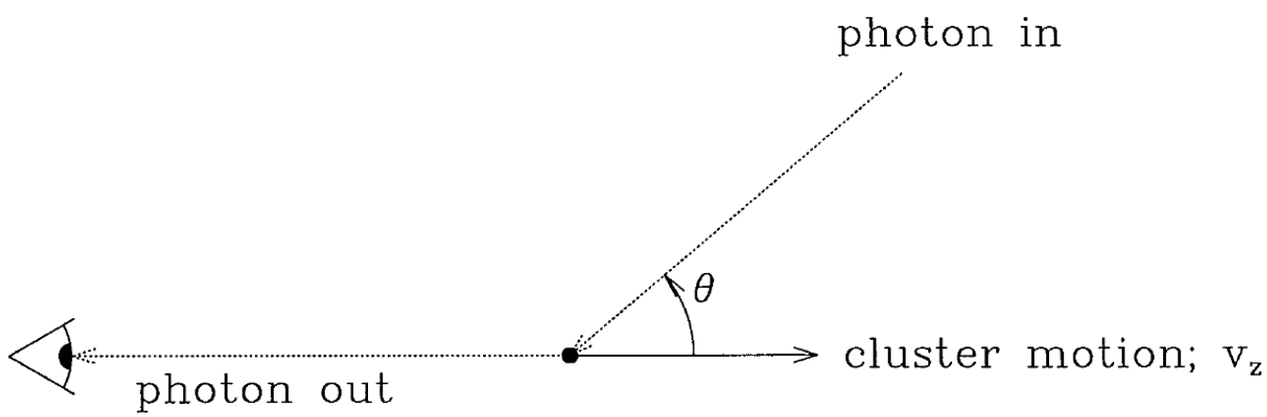

Fig. 12. The geometry for the discussion of the kinematic Sunyaev–Zel'dovich effect, as seen in the frame of an observer at rest in the Hubble flow.

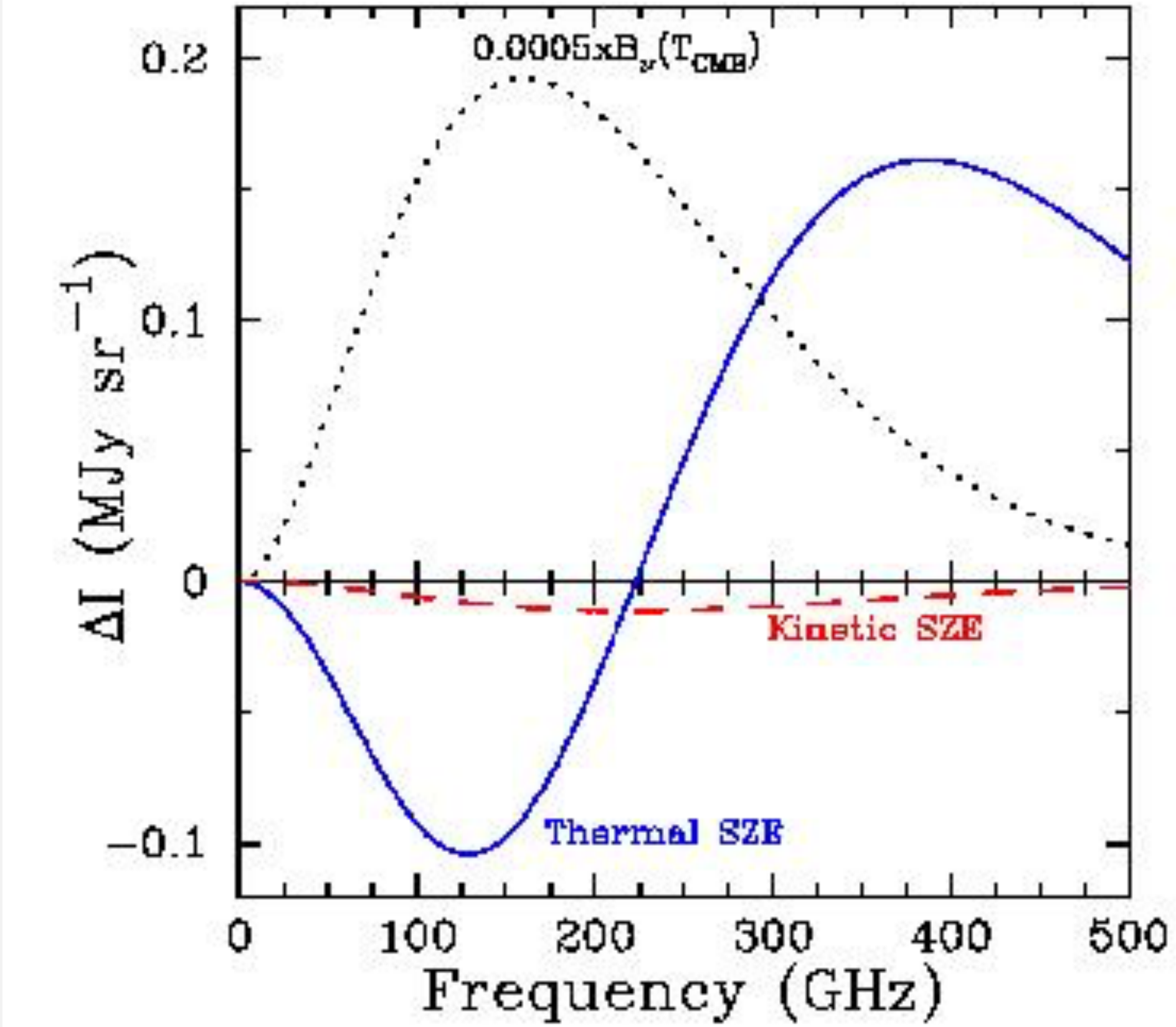
0.0005xB$_\nu$(T$_{CMB}$)
Kinetic SZE
Thermal SZE
0.2
0.1
0
−0.1
0
100
200
300
400
500
Frequency (GHz)
ΔI (MJy sr^{-1})